Journal of Engineering Mathematics **47:** 277–298, 2003.

Fluid flow through various branching tubes

F.T. SMITH[1], R. PURVIS[1], S.C.R. DENNIS[2], M.A. JONES[3], N.C. OVENDEN[4] and M. TADJFAR[5]

[1]*Department of Mathematics, University College London, Gower Street, London WC1E 6BT, UK;* [2]*Department of Applied Mathematics, University of Western Ontario, London, Ontario, Canada, N6A 5B7;* [3]*Courant Institute of Mathematical Sciences, 251 Mercer Street, New York, NY, 10012, USA;* [4]*Faculteit Wiskunde en Informatica, Technische Universiteit Eindhoven, Postbus 513, 5600 MB Eindhoven, The Netherlands;* [5]*Advanced Computing Center, Institute of Physical and Chemical Research (RIKEN), 2-1, Hirosawa, Wako-shi, Saitama, 351-0198, Japan*

Received 7 August 2002; accepted in revised form 27 August 2003

Abstract. In this part-review part-new work, studies on branching tube flows are described. These are based on modelling for increased flow rates as well as on direct numerical simulations and are motivated by applications to the cardiovascular system, lung airways and cerebral arteriovenous malformations. Small pressure differentials acting across a multiple branching are considered first, followed by substantial pressure differentials in a side branching, multiple branching or basic three-dimensional branching. All cases include a comparison of results between the modelling and the direct simulations. Wall shear, pressure variation, influence lengths, and separation or its suppression are examined, showing in particular sudden spatial adjustment of the pressure between mother and daughter tubes, nonunique flow patterns and a linear increase of flow rate with increasing number of daughters, dependent on the specific conditions. The agreement between modelling and direct simulations is generally close at moderate flow rates, suggesting their combined use in the biomedical applications.

Key words: arteriovenous malformations, branching-tube flows, multiple branches, slender geometry

1. Introduction

Branchings of fluid flow are extremely common throughout the human body and involve various complex geometrical configurations and flow conditions associated with different ranges of Reynolds numbers, pulsatility and wall flexibility. Branchings greatly affect the fluid dynamics and are common sites of disease. Many previous studies (*e.g.* [1–3]) address representative/modelled aortic or carotid branchings for instance in which typically one mother vessel bifurcates into only two daughters, with [4] commenting on early generation branches in the cardiovascular system and in the lungs. Networks due to successive branchings are also not uncommon, but their modelling to date has not allowed for complex local branching properties. These settings form one motivation for the current research.

The other main motivation is in the haemodynamics of cerebral arteriovenous malformations (AVMs) and surgical decision-making on their treatment. In an AVM a feeding artery undergoes an abrupt splitting into many thin daughter vessels (perhaps 20) with a tangled geometry which then drain into the venous system. In practice, there are often several arterial feeding vessels and several draining veins attached to each AVM, but a good starting point is the single-feed case. The AVM structure is observed to yield small vascular resistance overall which leads to a total blood flow rate or 'throughput' much larger than that normally occurring between the high pressure arterial and low-pressure venous systems. See [5–8]. AVMs repres-

ent a major life threat in the form of a stroke, especially to people aged under 50. The surgical procedures employed, in order to reduce the flow rate through the AVM, include clipping and glue casting, and are largely empirical, being founded on a wealth of experience and caution. It could be extremely beneficial to try to understand from a haemodynamical standpoint why these procedures are effective at lowering the flow rate and if possible how they may be improved upon. Branchings are of course also important in many other contexts *e.g.* those in the preceding paragraph, but the AVM context raises the central haemodynamical question of how the comparatively large flow rates are produced. Other major features are: the blood flow survives an expansion of arterial area in a typical AVM without flow reversal/choking; the inflow pressure is pulsatile whereas the outflow pressure is uniform; an AVM has a profound effect on the larger network of cerebral blood vessels. These features altogether raise new fundamental questions in haemodynamics.

Most of the branched flows of interest here are essentially laminar, with Reynolds numbers up to a few hundred, and can be taken often to be quasi-steady because of the short length scales near the branching and hence short typical times scales compared with the long-scale oncoming flow. Again, based on the estimates in [9,10], a predominantly inviscid model seems justified locally in most settings. This is in contrast to other works on one-to-two branching flows on a larger scale and related flows which include viscous effects, by [11–15], and likewise in contrast to longer-scale responses in the AVM model setting.

On networks, models have been proposed for the intracranial blood vessel networks, *e.g.* [16,17], incorporating an AVM model, and these also require improved understanding of the substantial influence from an AVM-like multiple branching on the total contained flow. Most studies on networks either overlook almost all the details of the haemodynamics at the individual branchings or use direct numerical simulation for just a few branchings. These studies include [16–21]. There are numerous other analytical or numerical works within the overall area, some of which overlap slightly with aspects of the present investigation, *e.g.* by [10,22,23]. Particularly noteworthy is the work in [10,24] which is used (*e.g.* see [21]) in modelling the lung airways for symmetric branchings (Weibel model, and see [18]) and is found to work very well within certain limits. Other basics of local branching are in [25].

Flows through multiple branchings, side branchings and others are of interest generally, then, in terms of the induced wall shear stress, pressure variation, influence lengths, flow reversal (separation) and total mass flux as well as certain specific issues below. The present investigations on branching flows arose from several biomedical projects. Analysis and computation are applied to model problems with the aim of providing greater physical understanding and perhaps rapid accurate calculations. The modelling, analysis and direct numerical simulations go very much hand-in-hand in the research, as will be seen in subsequent qualitative or quantitative comparisons throughout.

Direct numerical simulations of the Navier-Stokes equations are manyfold for branching flows [1–3,10,18–26]. Examples especially relevant in the current setting are in [18,21], the latter examining planar motion through two successive symmetric branchings, motivated by application to modelling of lung-airways flow; see also references mentioned earlier. The branching angles involved in [21] vary from zero to 70° and computations are presented for Reynolds numbers from 200 to 1200, which is a physiologically important range. Comparisons with their results are made later in this study. There are relatively few accurate direct simulations for more complex branchings.

The present aims are to study multi-branching (one mother to many daughters), obtain insight for several or many generations of branching and provide guidance on network interac-

tions; we also summarize theoretical modelling based on high throughput (*i.e.*, relatively high flow rates) but coupled with direct simulations by ourselves and others, along with comparisons. The work is partly review but partly new, specifically in terms of the new comparisons, the common features found, the new direct simulations on multi-branching flow and the new three-dimensional flow study. Overall, the approximations of high throughput are found to work well at Reynolds numbers above about 100 or even lower in practice [9,27–31].

Theoretical and computational aspects provide the focus in the following sections, it being suggested that their use together could be more beneficial for all the main biomedical contexts. The sections below also focus on central features of the projects involved. Section 2 considers the effects from small changes in mass flux or pressure differentials over the $O(1)$ length scale within a slender multi-branching geometry. The findings lead into the ensuing work in Sections 3–5, all of which investigate substantial $O(1)$ pressure differentials over an inviscid or a viscous length scale. Specifying the pressure differentials rather than mass fluxes seems more realistic in general although that is still open to debate. Again, small and substantial pressure differentials need defining: broadly 'small' corresponds to the majority of the mother tube flow (*e.g.* the velocities) being disturbed by only a small relative amount, whereas 'substantial' corresponds to the whole flow being altered by an $O(1)$ relative amount. Section 3 is on side branching, Section 4 reconsiders multi-branching under substantial pressure differentials and Section 5 is on a basic three-dimensional slender branching of one-to-two form. Most of these are for steady flow but unsteadiness is included in the side-branching study of Section 3. All cases in Sections 2–5 include a qualitative or quantitative comparison with a direct numerical simulation. Section 6 provides final comments.

Technical points. For high throughput there are usually two main length scales, which we measure here relative to the typical tube diameter. One is $O(1)$ and is associated with the tube geometry itself, so that the flow structure comprises an inviscid core with thin viscous wall layers if large-scale separation is precluded. The other major length scale is $O(\mathrm{Re})$, the flow development length, and corresponds to the viscous layers in effect filling the whole tube; usually that means an absence of upstream influence over this long scale (but see [27] or below). Both two- and three-dimensional branching-flow models are of concern here, the former being expressed in terms of suitably nondimensional velocities u, v along the tube axis and transverse respectively, corresponding stream function ψ, pressure p, Cartesian coordinates x, y and time t. The typical nondimensionalization is with respect to a representative incoming tube flow speed u_0, tube diameter a_0 and the density of the assumed incompressible fluid. In three-dimensional cases the non-dimensional third velocity component and coordinate are w, z respectively. The Reynolds number Re is $u_0\, a_0/\nu$ where ν is the kinematic viscosity of the fluid. The branchings considered herein have idealised shapes.

2. Multiple branchings with small pressure changes

This work on the influence of small pressure differentials briefly recapitulates [28] (the main points only) as that leads into the studies in the following sections, as well as into a new comparison with direct simulations in this section. The work also relates generically to several types of cardiovascular and cerebrovascular branching, including AVMs. It assumes a nonuniform incident velocity profile $u = u_0(y)$ with zero slip at the walls in the single mother tube upstream and a branching (starting at $x = 0$ say) into N daughter tubes downstream [28]. Here u_0 depends only on y and is positive between the upstream outer walls $y = 0, 2$. The

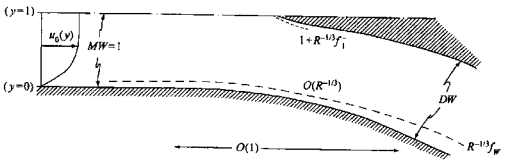

Figure 1a. Sketch of case for two large daughter tubes, with symmetry about $y = 1$ and with R denoting Re.The x axis is in the direction of the velocity u_0, and $x = 0$ at the start of the divider. Here $N = 1$, the mother half-width and daughter width are MW, DW respectively, and the wall shapes (divider, outer, in turn) are given by $f_1^-(x)$, $f_W(x)$ with x of order unity.

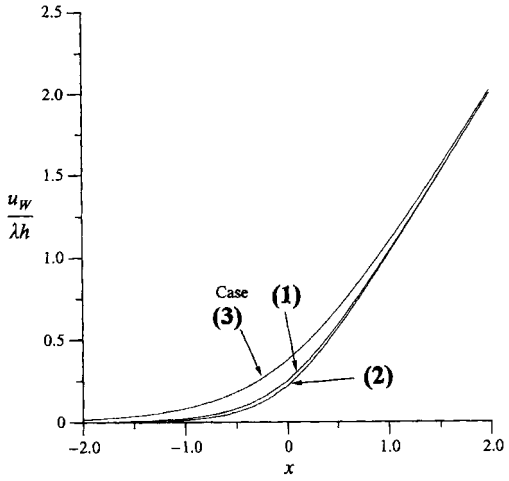

Figure 1b. Two large daughter tubes case. Slip-velocity results calculated from the inviscid core, for the three incident profiles of plane Poiseuille flow (1), uniform shear (2) and uniform velocity (3), with a wedged divider shape of angle $\propto h$.

planar geometry and flow are assumed symmetric about $y = 1$ for convenience, the overall pressure differentials as imposed from upstream to downstream are taken to be small, and the outer walls and daughter dividers are all nearly aligned. This, as shown in Figure 1(a) (and 2(a,c)), is consistent with a multi-branching flow structure for x of order unity comprising an inviscid core in the mother and daughter tubes along with thin $O(\mathrm{Re}^{-1/2})$ viscous layers on the dividers between the daughter tubes and an $O(\mathrm{Re}^{-1/3})$ viscous outer-wall layer, for large Re, where the divider thicknesses are taken to be of $O(\mathrm{Re}^{-1/3})$. The scaling here follows from the inertial-viscous balance $u\,\partial/\partial x \sim \mathrm{Re}^{-1}\partial^2/\partial y^2$ near the outer wall where $u \sim \lambda y$, the $O(1)$ constant $\lambda \equiv u_0'(0)$ denoting the scaled wall shear upstream.

The core-flow effect is linear, in keeping with the relatively small changes produced by the small pressure differences and near-alignment, so that $u - u_0(y)$ is small and equal to $\mathrm{Re}^{-1/3}\tilde{u}(x, y)$ say with $\tilde{u}$ of $O(1)$. This $\frac{1}{3}$ scaling is due to the divider thicknesses. Hence the small-perturbation system

$$u_0(\partial^2/\partial x^2 + \partial^2/\partial y^2)\tilde{\psi} = u_0''\tilde{\psi} \tag{2.1a}$$

applies, where $\tilde{u} = \partial\tilde{\psi}/\partial y$, with the stream function perturbation $\tilde{\psi}$ being zero far upstream and along $y = 0, 1$ (except possibly for $y = 1,\ x > 0$). Also, if the divider walls are given by $y = y_n + \mathrm{Re}^{-1/3}f_n^{\pm}$ for $n = 1$ to N, with y_n, $f_n^{\pm}(x)$ prescribed, while c_n denotes the scaled mass flux value for the nth. divider, then

$$\tilde{\psi} = -u_0(y_n)f_n^{\pm}(x) + c_n \quad \text{at} \quad y = y_n \pm . \tag{2.1b}$$

The condition (2.1b) is the tangential-flow constraint. The geometry of the branching is prescribed by the scaled divider shapes f_n and scaled outer wall shape f_W. The internal viscous

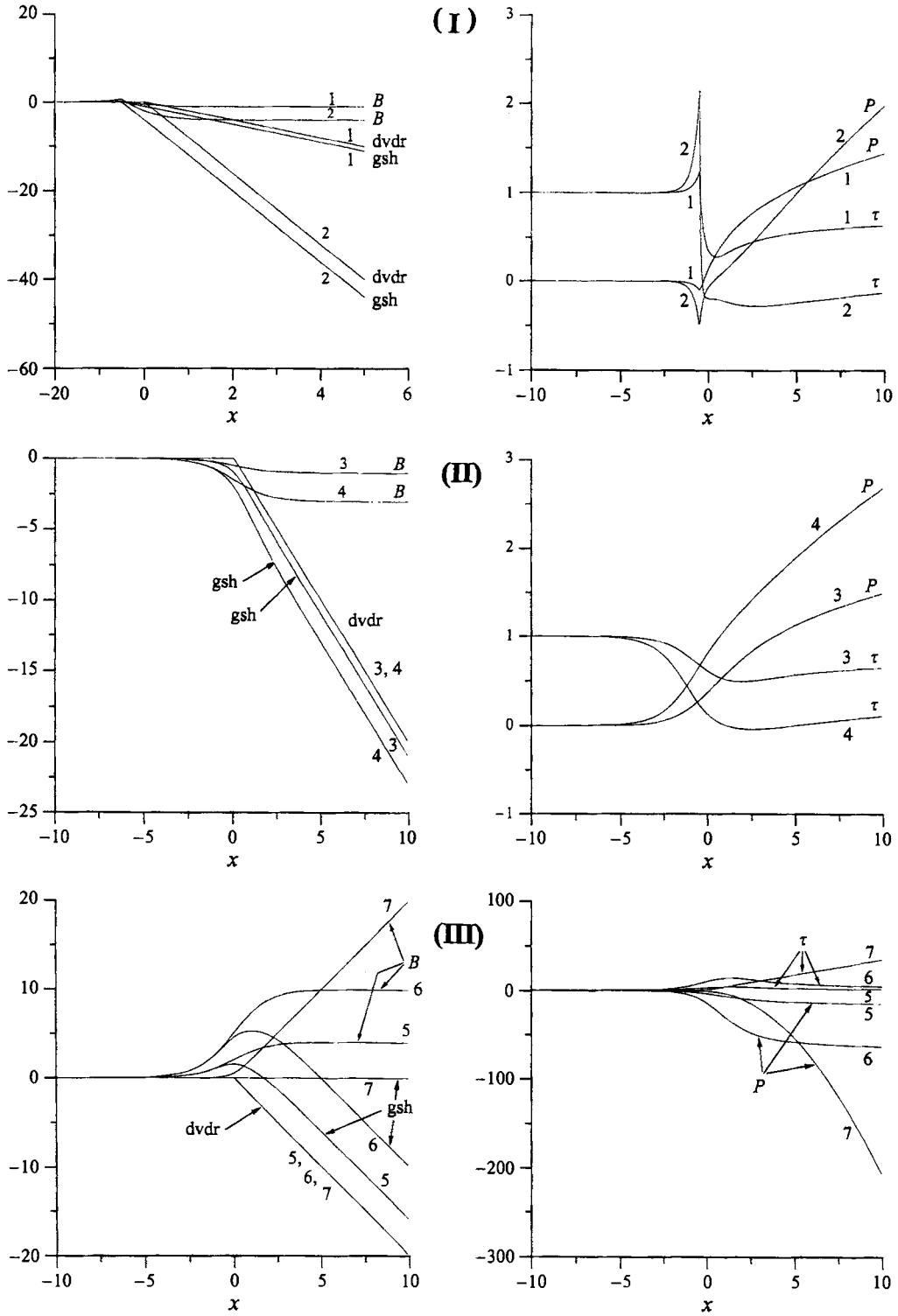

Figure 1c. Two large daughter tubes case. Viscous wall-layer results computed in seven cases 1–7 (in each the divider shape and wall shape are specified as shown graphically), showing the induced pressures, wall shears and effective viscous displacements, along with the prescribed divider (dvdr) and wall shapes (gsh) for comparison.

layers and the outer wall shape $f_W \equiv f_0^+$ alike have negligible influence so far. The solution for $\tilde{\psi}(x, y)$ yields a scaled slip velocity u_W equal to $\tilde{u}(x, 0)$, *i.e.*, $\partial\tilde{\psi}/\partial y(x, 0)$, at the outer wall.

The outer wall-layer flow is nonlinear. It has $y = \mathrm{Re}^{-1/3}(Y + f_W(x))$ and u, p are $\mathrm{Re}^{-1/3}U$, $\mathrm{Re}^{-2/3}P(x)$ to leading order, leaving the boundary layer system

$$U = \frac{\partial\Psi}{\partial Y}, \; U\frac{\partial U}{\partial x} - \frac{\partial\Psi}{\partial x}\frac{\partial U}{\partial Y} = -P'(x) + \frac{\partial^2 U}{\partial Y^2} \tag{2.2a,b}$$

with $\partial P/\partial Y$ zero from the normal momentum balance. The boundary conditions are

$$U = \Psi = 0 \text{ at } Y = 0, \tag{2.2c}$$

$$U \sim \lambda\{Y + B(x)\} \text{ as } Y \to \infty, \quad B \equiv \lambda^{-1}u_W(x) + f_W(x), \tag{2.2d}$$

$$(U, \Psi, P) \to (\lambda Y, \frac{1}{2}\lambda Y^2, 0) \quad \text{as} \quad x \to -\infty, \tag{2.2e}$$

in view of the no slip requirement at the outer wall and matching with the core and upstream motions. The system allows separation/flow reversal, if it occurs, to be regular since P is an unknown.

The argument extends to three-dimensional branchings as described in [28], but these induce a logarithmic effect (where any divider meets the outer wall) in the core which limits the applicability of the theory in the present setting: compare Sections 3 and 5.

2.1. Results

We focus attention on three specific planar branchings (i)–(iii) for the remainder of this section.

(i) The first is for two large daughters with symmetry about $y = 1$, see Figure 1(a). In this branching the core problem (2.1a,b) can be solved directly by using a Fourier transform in x, to enable the influences of geometric shapes, the incoming velocity profile, the daughter width DW relative to the mother width MW, and so on, to be examined. The core solution produces the inviscid slip distributions u_W shown in Figure 1(b) for several different u_0 profiles and a given divider shape, a noteworthy feature being the similarity between the distributions. Feeding u_W into the viscous wall-layer problem via (2.2d) then yields the results for outer wall shear and pressure shown in Figure 1(c). These are for several distinct cases 1–7, in each of which the shapes of the central divider ($dvdr$) and the wall (gsh) are indicated. Cases 1, 2 are examples that have an overall area expansion due to the branching which provokes an adverse pressure gradient and shear reduction downstream, leading in one case to outer-wall separation/flow reversal. Cases 3, 4 have area expansions which are different in geometrical detail, again causing a trend towards flow reversal with a relatively long recirculating eddy downstream, but upstream the effects are opposite to those of cases 1, 2. Cases 5–7 yield an overall contraction of area, which forces a favourable pressure gradient and wall-shear increase downstream.

(ii) The second specific branching is for a small daughter as shown in Figure 2(a), where α is the daughter width scaled relative to the mother width. The core solution yields the results for u_W/c_1 presented in Figure 2(b), as α is varied. The results confirm in particular that most of the change in u_W occurs within a short distance $O(\alpha)$ of the daughter mouth when α is small, *e.g.* 0·1 or less, the other distinguished length scale being $O(1)$ ahead of and after the

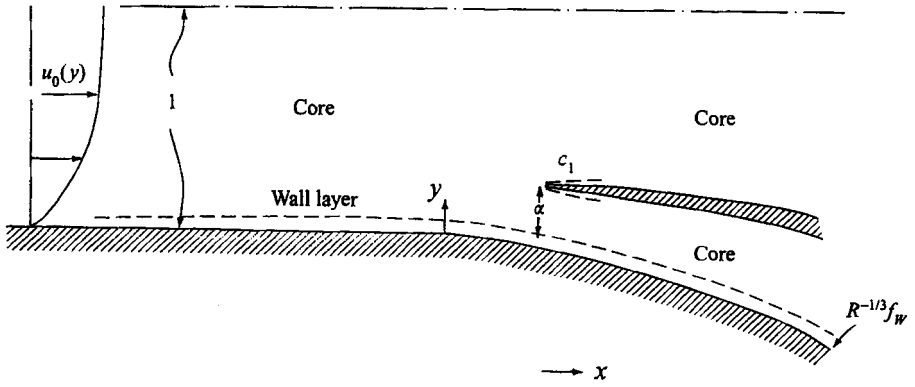

Figure 2a. Branching for an increasingly small daughter tube, of width α. The flow structure, with R denoting Re again.

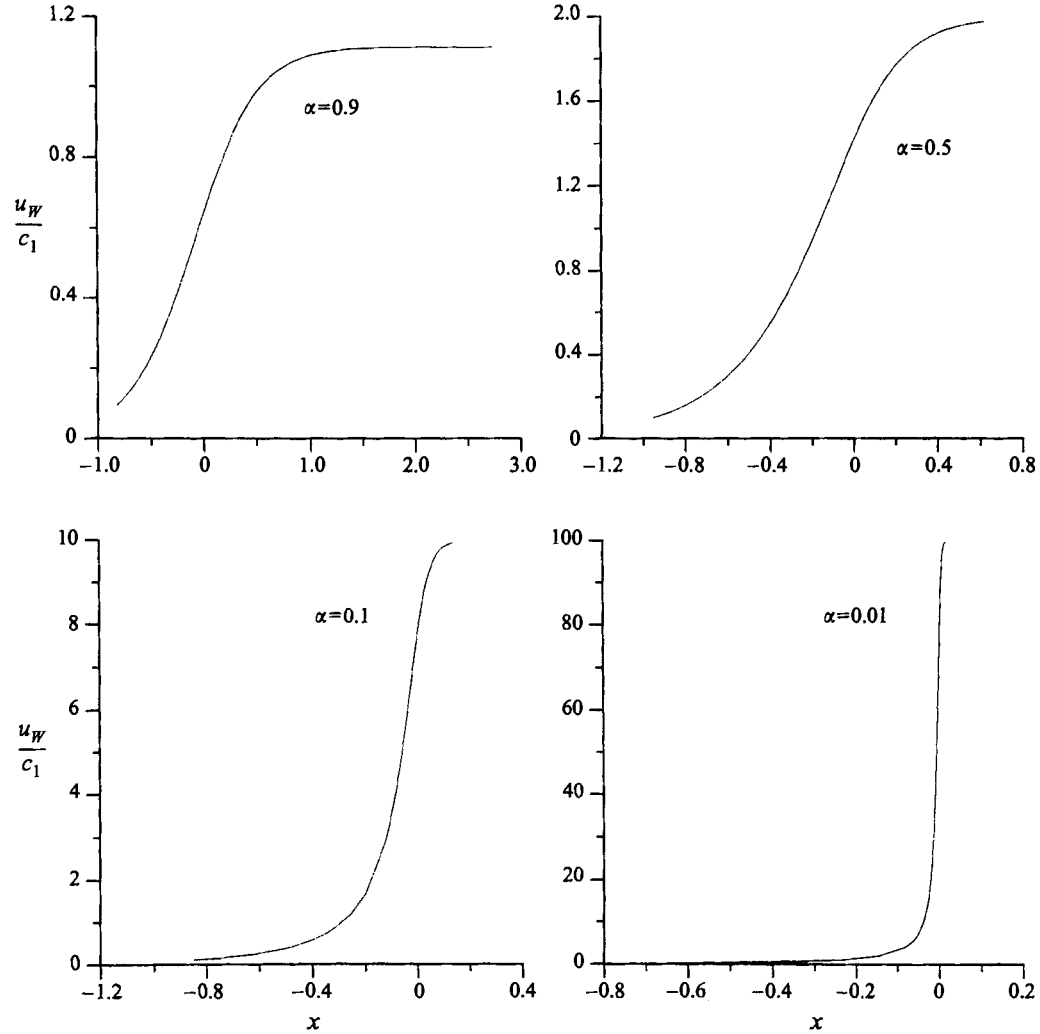

Figure 2b. Branching for an increasingly small daughter tube, of width α. Computed slip velocity for various α values from the inviscid core; c_1 is the scaled mass flux into the daughter tube.

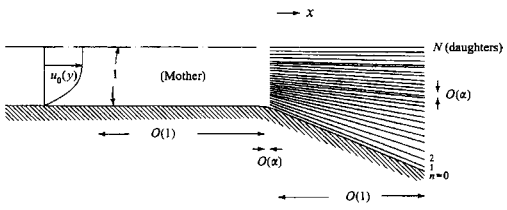

Figure 2c. Branching with many small daughters. For general incident profile u_0, the flow structure with large N, small α, including the main three streamwise length scales of the mother, mouth and daughter flows and the two lateral length scales.

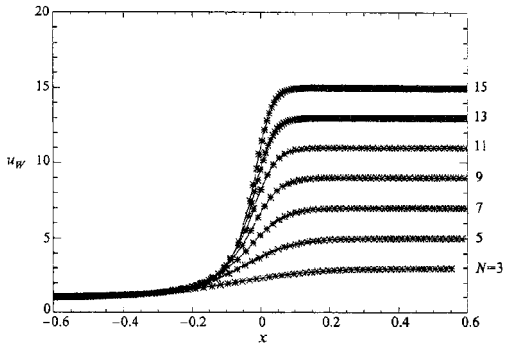

Figure 2d. Slip velocity for the case of branching with many small daughters as N is varied.

mouth. Over the latter global scale the full profile u_0 has effect but the daughter acts as a sink-like disturbance at the wall, whereas over the $O(\alpha)$ local scale the details of the daughter mouth are apparent and only the incident shear flow λy drives the local flow. Properties in this branching (ii) prompt the work in Section 3.

(iii) Third is the branching for many small daughters as illustrated in Figure 2(c), where $N \gg 1$ but $\alpha \ll 1$. Now the solution in the inviscid core gives in detail the u_W results in Figure 2(d) as N increases: u_W is plotted instead of u_W/c_1 for clarity. Here again length scales of orders unity and α operate. The mother flow ahead of the multi-branching at $x = 0$ poses a half-range problem in which the pressure at $x = 0-$ is given, being prescribed by the individual daughter flows each of which tends to act alone; between them is the $O(\alpha)$ region at each daughter mouth. Associated wall-layer features are shown in [28], indicating in particular that this multi-branching can permit enhanced turning of the overall flow without significant flow reversal. The findings for (iii) prompt the study in Section 4.

2.2. COMPARISONS

Qualitative comparisons can be made with the direct simulations in [21] over their Re-range 200 to 1200, for a fixed geometry with typical turning angle $\alpha = \pi/6$ at successive wedge-like branchings. At Re = 200, 500 confined recirculatory eddies are found in their Figure 3 at most of the outer walls after each branching, and the eddy lengths increase with increasing Re. In contrast, the wall shear is enhanced both on the outer wall ahead of the branching and on the inner divider wall. The reversed-flow trend is such that at Re = 900, 1200 one outer-wall eddy extends downstream to the next branching and joins with the next outer-wall eddy, while others continue to elongate. (A new eddy also forms at Re of 1200). These features of the simulations seem supportive of the theory for branching type (i) which does indeed predict increased outer-wall flow reversal as Re increases; see also [21, Figure 4]. The theory also predicts (*e.g.* see Figure 1(c)) enhanced wall shear upstream of branching and on the dividers, as in the simulations [21]. Moreover the extra turning produced by successive branchings in [21] without excessive reversals arising also, is in keeping with the theory for (iii) above. The

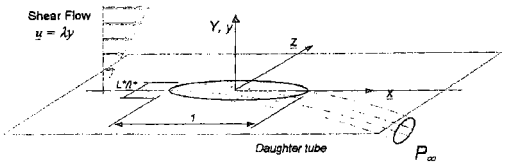

Figure 3a. The flow configuration for streamlined branching of a relatively small daughter from a mother tube, with incident shear flow, in nondimensional form.

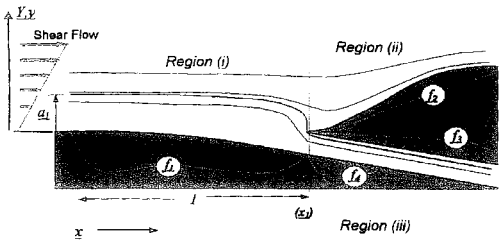

Figure 3b. As in Figure 3a, but for steady or pulsatile planar motion, showing the viscous regions (i)–(iii) and the wall shapes $f_1 - f_4$.

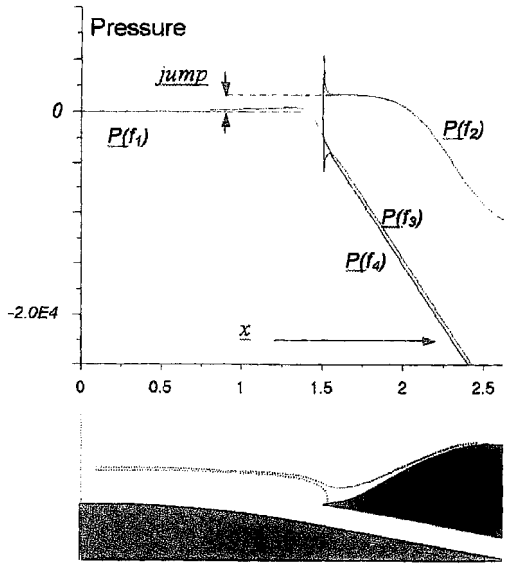

Figure 3c. A direct simulation for the geometry shown. Here Re = 222.

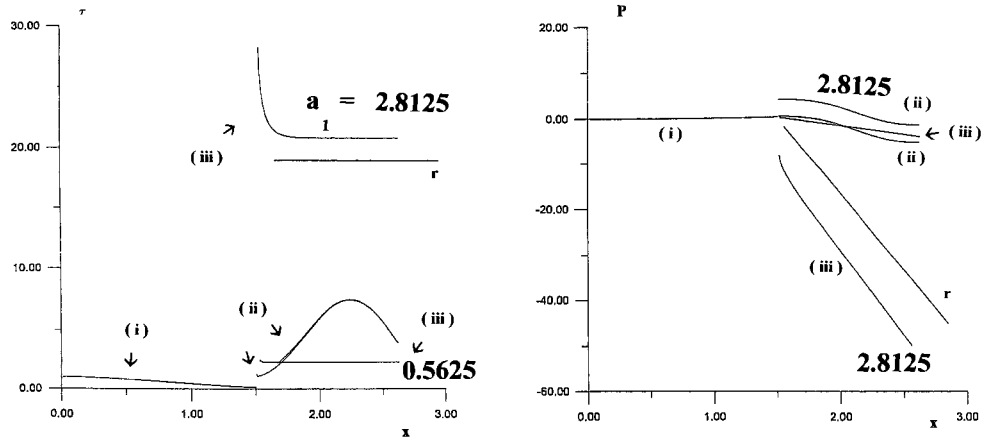

Figure 4. Planar model results for side-branching. In (a),(b): shear τ at walls f_1, f_2, f_4 and pressures P versus x, in regions (i)–(iii) respectively, for two values of a_1. Comparisons with limit predictions (denoted by r) are included.

comparative smallness of the critical Re for flow reversal, about 100, for an α value of $\pi/6$ in [21] is not inconsistent with the predicted $O(\mathrm{Re}^{-1/3})$ scale for α.

3. Side-branching with substantial pressure changes

The study here of slender side-branching stems from the special case (ii) in the previous section and again has potentially wide generic application. The work is based on [27] and is presented, albeit in brief, as it connects with that in the next section as well as with (ii)

above. Now however the pressure differences imposed are taken to be relatively substantial and the size of the small daughter or side-branch is reduced such that it all lies within the viscous near-wall layer as in figure 3(a,b). The essential difference in modelling between smaller and more substantial pressure changes, in the present setting, is that here a viscous-inviscid balance of effects describes the motion almost everywhere. Figure 3(a) shows a three-dimensional side branch, while Figure 3(b) shows the two-dimensional case, with the mother-flow regions (i), (ii), in the present nondimensional form based on the incident shear and the main streamwise length scale of the branching . The incident mother shear flow is uniform because of the near-wall position and size of the daughter. The imposed pressure within the daughter at some position $x = x_2$ downstream of the daughter entrance x_1 is denoted by P_∞, the mother pressure upstream being taken as zero, and $f_1 - f_4$ are the known normalized wall shapes, again in coordinates x and normalized y or Y, whereas the scaled thickness a_1 of mother fluid that is entrained into the daughter is unknown. The constants λ, L^*/ℓ^* denote the normalized shear and a ratio of the daughter-mouth dimensions respectively. Figure 3(c) presents a result from a direct simulation [27] at a moderate value of Re, showing the wall pressures. Most noteworthy is the apparent jump or rapid spatial change in pressure close to the mouth of the side-branch.

The explanation for the jump is as follows. For sufficiently large Re the slender-layer equations (2.2a,b) hold almost everywhere, subject to standard boundary conditions of no slip at each wall, and these suggest parabolic dependence, in the direction forward from the uniform-shear condition given upstream. Yet such a parabolic dependence on its own must usually violate the required downstream condition

$$P^- = P_\infty \quad \text{at} \quad x = x_2 \tag{3.1}$$

in the side branch, in which the pressure is P^-. The only resolution for this is that a discontinuity (jump) has to be present, specifically at the mouth $x = x_1\pm$, achieved by means of a local essentially inviscid Euler zone which conserves mass and pressure head,

$$\Psi \text{ and } P + \frac{1}{2}U^2 \text{ are conserved,} \tag{3.2}$$

along streamlines; then P, U^2 individually can jump across the zone ($x \to x_1\pm$). The jump here is supported by the local configuration of the surfaces f_1, f_3, f_4 combined with the incident shear. A jump cannot be sustained across any station x other than x_1.

The model system incorporating (3.1),(3.2), and thus predicting jumps in P and wall shear τ_W or τ, was solved numerically in two and three dimensions by rapid forward marching, sample results being given in Figures 4, 5 for steady planar motion. The two cases shown in the mother and side-branch solutions for τ, P in Figure 4 are for two different values of the entrainment parameter a_1. Also presented are analytical results [27] for comparison. Figure 5(a) then shows comparisons with direct simulation results [27] for pressure and wall shear at moderate Re for an individual case, while Figure 5(b) covers a range of cases (corresponding to different entrainment values) according to the model and compares with the direct simulation values obtained for two of those cases. The agreement is encouraging throughout.

The study in [27] also includes unsteady, three-dimensional and higher suction effects. This last effect provokes a sink-like behaviour at the branch mouth, the sink strength increasing with P_∞ and hence with a_1 and gradually generating substantial upstream influence. The influence is favourable, in the sense of reducing or suppressing any upstream separation.

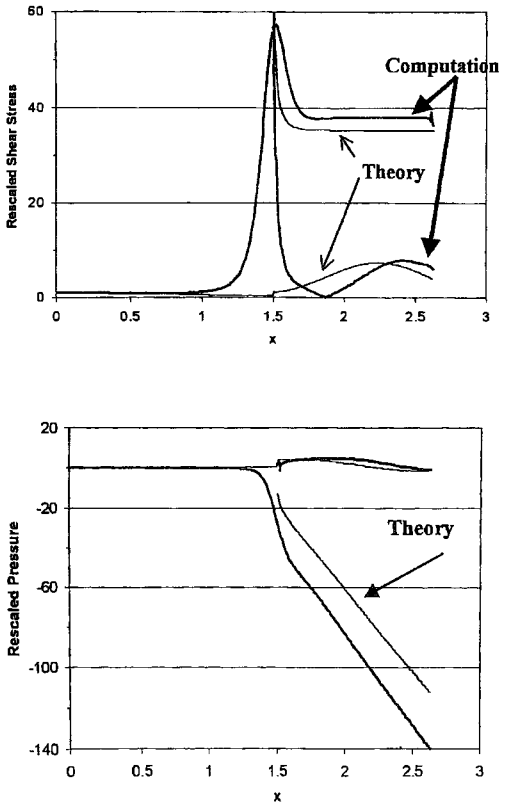

Figure 5a. Direct numerical simulations of the Navier-Stokes equations for side-branching. Wall shear stress, wall pressures. This includes results from the theory (modelling), for comparison.

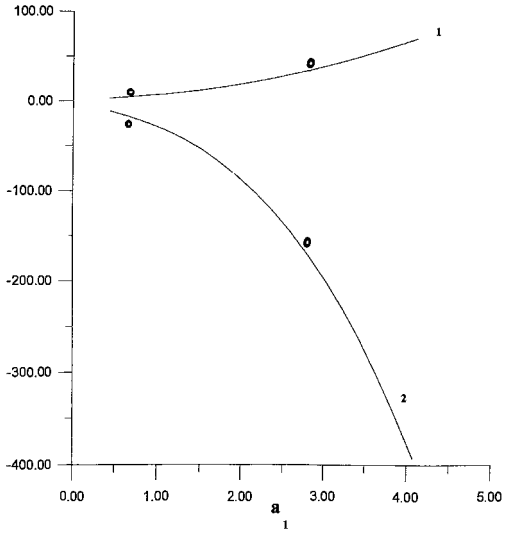

Figure 5b. Direct numerical simulations of the Navier-Stokes equations for side-branching. Further comparisons: theoretical results for end shears τ_∞ and pressures P_∞ (labelled 1,2 in turn) in the daughter side-branch (iii) as a_1 varies. This includes values from simulations, shown as circles.

Downstream separation allows some fluid particles to flow past the side-branch before being dragged back into it.

4. Multi-branching with substantial pressure changes

Here the scaled pressure differentials are $O(1)$ and the local geometry is not necessarily slender, by contrast with the branching flows studied in Section 2. This account again builds on the two length scales described in Section 1 but the focus is on the local $x \sim 1$ scale. The biological/medical motivation is mainly in the application to AVM haemodynamics.

The theory in [9] is for planar flow in the branching geometry of Figure 6(a). In nondimensional terms, a single mother tube, of width 1 and containing fully developed incident flow of unknown total mass flux λ, branches locally into N daughter tubes of total width A ('area') at large positive x; in the figure N is 5. The exit velocities u_1 to u_N in the daughters are unknown. The branching shape involves arbitrary $O(1)$ slopes and is prescribed, as are the daughter pressures π_1 to π_N downstream, which are measured relative to the upstream mother

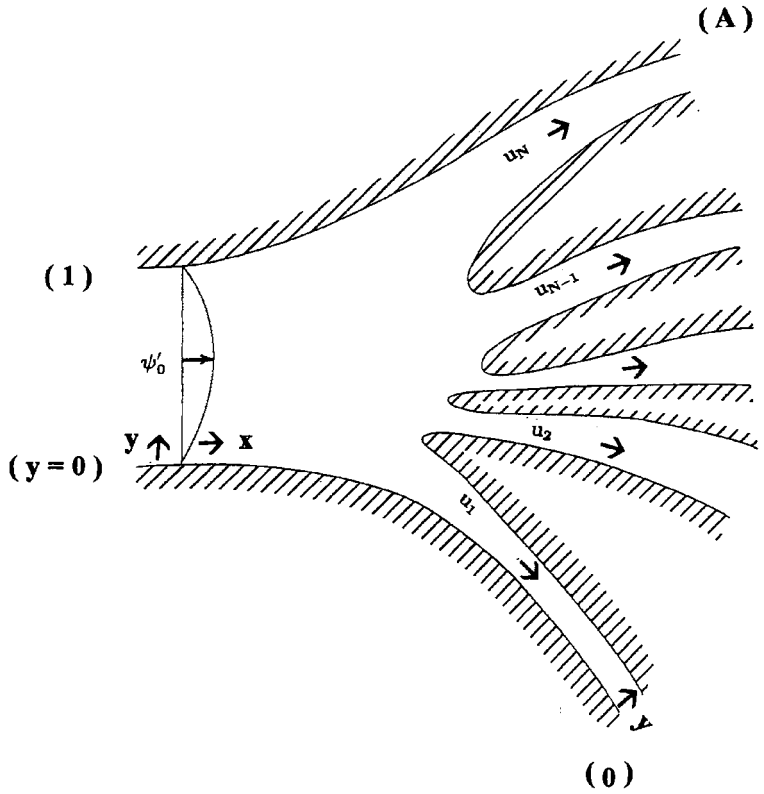

Figure 6a. Multi-branching with substantial pressure changes: model. Sketch of the branching flow from the mother velocity profile $\psi_0'(y)$ to N separate daughter profiles u_i downstream, with y measured laterally across each tube. In this case $N = 5$.

pressure. The latter is taken as zero. The orders of magnitude point to an inviscid response in the absence of significant separation.

Conservation of mass and pressure head are applied in each daughter, effectively as in (3.2), to determine λ under various area and pressure settings by means of a set of nonlinear recurrence relations and ordinary differential equations, with all the u_i for $i = 1$ to N being assumed positive. In consequence, the problem takes the form

$$A = \sum_{i=1}^{N} \int_{\psi_i^-}^{\psi_i^+} \frac{\mathrm{d}\psi}{\{\psi_0'(\psi_0^{-1}(\psi))^2 - 2\pi_i\}^{1/2}}, \tag{4.1}$$

where the size of the incident stream-function profile ψ_0 is to be found (the factor λ) together with the stream-function values $\psi_i^{\pm}$ on the walls of each daughter. The calculated response of λ as the prescribed area A is varied is given in Figure 6(b) for two types of pressure settings. The first has all the pressures π_i being negative, in which case a unique non-separated flow is predicted for any N throughout the interval $0 < A < 1$; the figure shows results for a range of N values along with asymptotes labelled I–III which stem from (4.1) for $A \to 0$, $A \to 1$, $N \to \infty$ respectively and provide a comparison. This type allows no solution if A is unity since the implied increase in u^2 and hence u is then incompatible with the total mass-flux requirement. The second type has at least one π_i being positive and that leads to restrictions on the left and right as non-separated flow is found to be impossible if A is too small or too

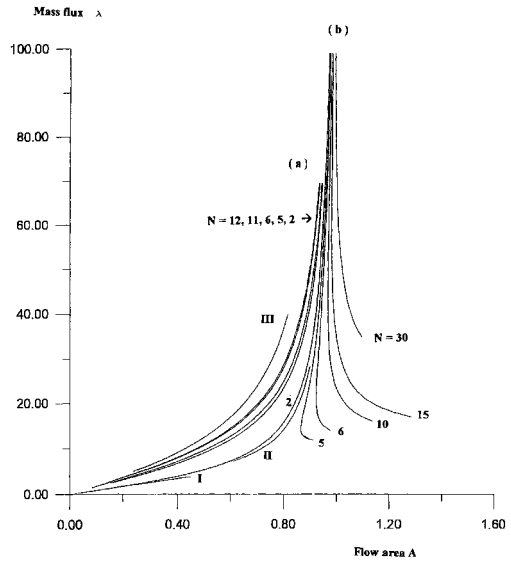

Figure 6b. Multi-branching with substantial pressure changes: model. Flow rate λ versus flow area A, for two π_i pressure distributions, with equal daughter areas and various N. Curves I-III are asymptotes. Pressures π_i are (a) $(-1, -6, -5, -6, -5, \ldots, -1)$; (b) $(-1, -1, 4{\cdot}5, 5{\cdot}5, 4{\cdot}5, 5{\cdot}5, \ldots, -1, -1)$.

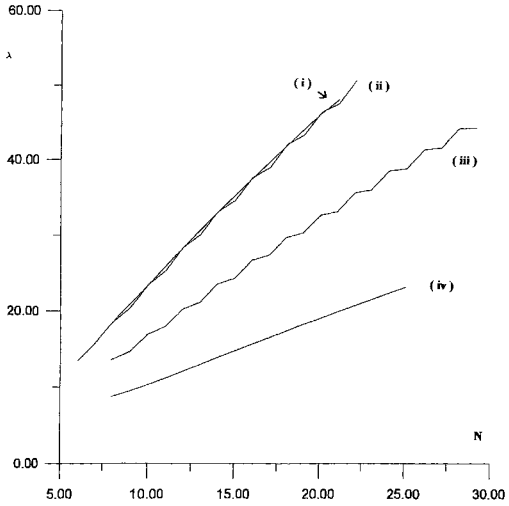

Figure 6c. Multi-branching with substantial pressure changes: model. For $A = 1$, mass flux λ against N in four cases each with equal daughters: $\pi_i = (-1, -1, b, c, b, c, \ldots, -1, -1)$ for b, c values of (i) 5, 5, (ii) 4·5, 5·5, (iii) 3, 4, (iv) 2, 2.

large; non-uniqueness can also arise then, as indicated in our Figure 6(b) and in [9, Figure 3] which demonstrates the notably different flow profiles predicted downstream. Concerning the restrictions above, in practice the flow may separate substantially or the velocity u_i may be reversed for some i values, negating the above analysis: see direct simulations below and the comments at the end of the paper. Figure 6(c) shows the dependence of λ on N for given pressure settings all of the second type and given area A, in four cases (i)–(iv). A remarkable feature is the linear increase of the total flux λ with increasing number of daughters N, in every case, for N above about 4. This and the asymptotes mentioned previously are analyzed in [9].

In broader terms, for instance in a complete AVM model, the π_i values themselves are governed by interaction between the shorter-scale inviscid problem above and the viscous development over the longer $O(\mathrm{Re})$ length scale (Section 1). This feedback is akin to that in the side-branching studied in Section 3, and [9] investigates one example of it.

Direct simulations were performed more recently to test some of the predictions above. The method is described in Appendix A. Sample results are given in Figure 7(a–c) and further ones are to be reported in [30]. Figure 7(a) has a moderate Re value and all the downstream daughter pressures except one are below the upstream mother pressure. The single daughter with a raised pressure is found to yield reversed flow in that daughter alone, as might be expected physically. Figure 7(b), again with a moderate Re, has a different distribution of downstream pressures but again only one is above the mother value. Nevertheless, forward flow is now produced in every daughter *including* the one with raised pressure. The reason lies with the comparatively low pressures in the other daughters in this case which generate

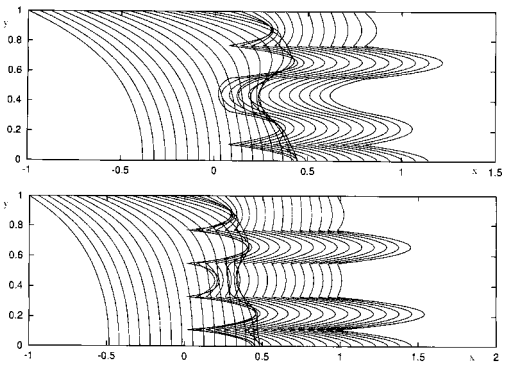

Figure 7a and Figure 7b. Multi-branching with substantial pressure changes: direct simulations and comparisons. (a) Streamwise velocity profiles at Re $=$ 50 for a symmetric case with $N = 9$ branches. Upstream pressure p is set to be 1 while downstream $p = -1, 0, 2, -1, -1$ in turn from top to bottom. Axes: x horizontal, y vertical. (b) As (a) but with downstream pressures given by $p = -1, -4, 1.5, -5, -5$ in turn.

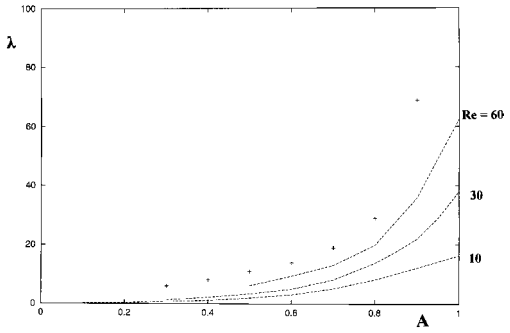

Figure 7c. Multi-branching with substantial pressure changes. Comparisons of mass flux at Re $= 10, 30, 60$ ($---$ from simulations) with the model analysis ($+$) (see Figure 6(b)'s case (a)), for varying downstream areas. Here $N = 11$ and the downstream pressures are $p = -1, -6, -5, -6, \ldots, -5, -6, -1$.

momentum at order-one x values sufficient to drive fluid into the raised-pressure daughter, *i.e.*, almost the 'wrong way' based on an overall pressure argument. We note that the daughter pressure conditions here are perhaps imposed at a relatively short distance downstream in terms of the longer scale mentioned in the preceding paragraph. Results from direct simulation and modelling are compared in Figure 7(c) over a range of areas A, showing fair agreement as Re increases.

5. Three-dimensional branching with substantial pressure changes

The three-dimensional branching geometry and flow are now taken to be slender (see [31]), while the $O(1)$ pressure differentials are imposed over the long viscous length scale. We focus on the archetypal problem of steady flow through a Y bifurcation of small angle, *i.e.*, a one-to-one branching of a mother into two diverging daughters. Previous theoretical studies [11–13,15,28] concentrate mostly on the shorter length scale (Section 1), usually with zero bifurcation angle.

The slender-flow equations on the $O(\mathrm{Re})$ length scale where $x = X\mathrm{Re}$ (denoting distance along each tube or branch) and $(v, w) = (V, W)/\mathrm{Re}$ are, as in [11],

$$u_X + V_y + W_z = 0, \tag{5.1a}$$

$$u u_X + V u_Y + W u_Z = -p_0'(X) + \nabla^2 u, \tag{5.1b}$$

$$u V_X + V V_y + W V_z = -p_{1y} + \nabla^2 V, \tag{5.1c}$$

$$u W_X + V W_y + W W_z = -p_{1z} + \nabla^2 W, \tag{5.1d}$$

where ∇^2 now denotes $(\partial_y^2 + \partial_z^2)$ and $u, V, W, X, y, z, p_0, p_1$ are $O(1)$. The pressure is $p_0 + \mathrm{Re}^{-2} p_1$, with p_0 being independent of y, z from the cross-sectional (y, z) momentum balance.

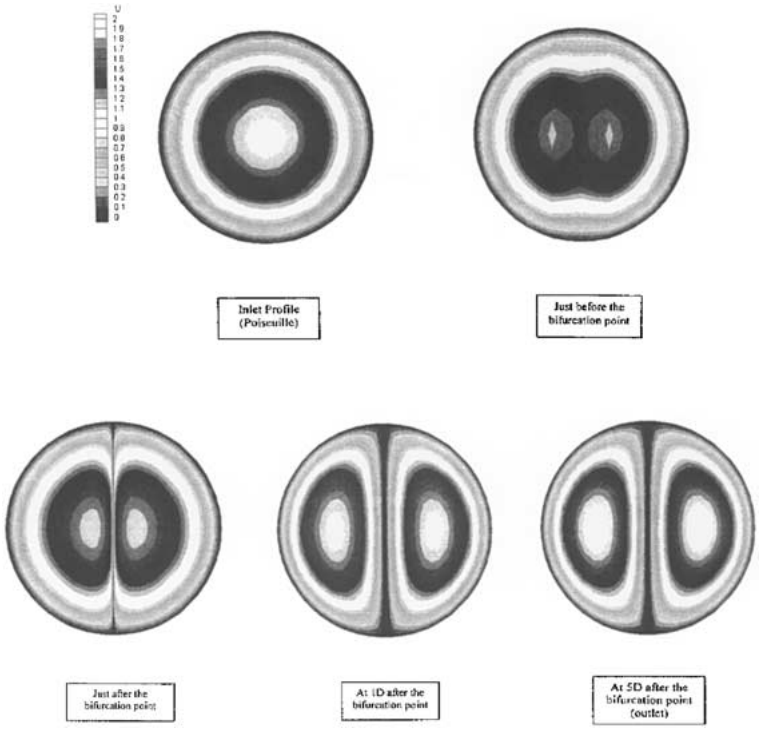

Figure 8. Three-dimensional branching from a circular mother to two semi-circular daughter tubes. Direct-simulation results in the cross-plane at Re = 100.

There is no upstream influence on this scale provided that flow symmetry is preserved (non-symmetry by contrast provokes local adjustments as in Sections 3, 4), u remains positive and the total flux is given (see below). The incident mother profile acts as a starting condition for each daughter flow, which can be determined in parabolic fashion by marching forward in X. Solutions of (5.1a–d) subject to standard no-slip conditions at the walls have been calculated by finite differencing applied to u, V, W and the cross-sectional vorticity function [11], p_1 being eliminated by cross-differentiation in (5.1c,d). In principle any cross-sectional shape can be dealt with in the numerical scheme that has been developed; the calculations are based on a displaced Cartesian grid coupled with interpolation at the walls. The program is run with either the total mass flux prescribed or an upstream-to-downstream pressure differential prescribed, the latter being accommodated by iteration.

Direct simulations were also conducted, as detailed in Appendix B. See Figure 8 which shows results for a circular mother and two semicircular daughters.

Comparisons between the simulations and the slender-flow results are summarized in Figure 9. This plots the normalised shear stress on the midway line of the divider against normalized distance along the daughter, for the circle-to-semicircle bifurcation, according to the theory and simulation at Re of 100. The agreement is quite close. Continued computations and comparisons are planned [31] for more divergent daughters to increase the potential application.

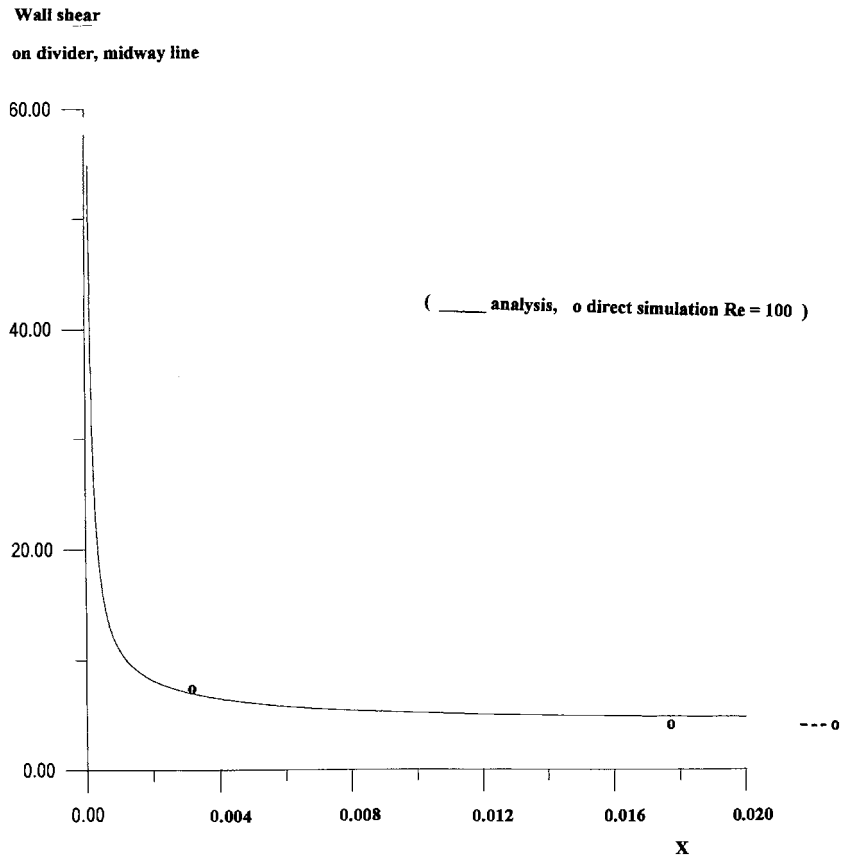

Figure 9. As Figure 8 but comparing results of analysis/modelling (solid, universal curve) and direct simulation at Re = 100 (circles), for normalized wall shear on the divider midway line plotted against scaled distance X within a daughter. Again X is measured from its zero value at the start of the divider.

6. Conclusions

We have examined the effects of both small pressure differentials, in multi-branching (Section 2), and substantial pressure differentials, in side-branching and a basic three-dimensional symmetrical branching as well as multi-branching (Sections 3–5). This has been through a combination of theory and computation throughout. That combination, partly from existing works and partly from new work, is encouraging in terms of building up more understanding over a broad range of flow rates and pressure conditions. The flow features found include abrupt spatial adjustment of the pressure between mother and daughter tubes, nonunique flow patterns and a linear increase in throughput as the number of daughters is increased.

The theory/modelling may involve significant simplifying assumptions and hence limitations, but direct simulation although powerful likewise has limitations, for example on the sensitivity to input data of wall shape, end conditions and boundary conditions which are difficult to prescribe in practice, and on the handling of one case (patient) at a time. Theory and direct simulation together seem to offer much more however. The theory yields parameter ranges, generic properties, wider applicability in principle and extra insight, suggesting that the combination of theoretical modelling and direct simulation may improve the chances of increased progress.

Concerning detail, there is some dependence on the specific conditions of course. A sample detailed point on specific conditions concerns the behaviour $Q \sim \kappa N$ of the mass flux Q as the number N of daughters increases, in the context of Section 4, where κ is a constant. In the two cases studied with downstream pressures $(-1, -1, b, \ldots, b, -1, -1)$ the value of κ can be shown [9] to be $6b/\sqrt{8}$, which agrees well with the numerical results, but the pressure constant b must be positive, and generally the dependence of the flow solution on the thin nonlinear layers at the outermost walls is delicate. Other aspects peculiar to the different branchings are clear in the preceding sections.

It is perhaps still too soon to apply the modelling direct to cardio- or cerebro- vascular flows, especially in a patient-specific sense. Further research is needed on the modelling side, *e.g.* to broaden the range of conditions covered, such as for other pressure differences, to accommodate more three-dimensional effects including swirl, multi-branching, and branching through successive generations or even a network, and possibly to incorporate more realistic vessel shapes. The branching-flow symmetry present in the three-dimensional flow study of Section 5 is significant in the modelling in the sense that the full nonsymmetric three-dimensional case is much more difficult to analyze, owing to local pressure jumps akin to those of Section 3. One promising approach there could be based on the flow structure described in Section 3 but incorporating so-called opposite wall effects [27]. More complex geometry also poses a considerable challenge. Work has begun on applying the three-dimensional slender-flow approach of (5.1a–d) to less idealized shapes, on upstream-shaping effects (compare [18]) and on extending the comparisons of Sections 4, 5 to encompass nonzero angles in both the simulations and the modelling. Concerning networks and their related interactions, an obviously important role is played by the two main long (viscous) and short (predominantly inviscid) length scales, *i.e.*, global and local respectively; this is seen in Section 3 which has both long and short scales, linked by pressure adjustments, in Section 4 which focusses on the short-scale response, and in Section 5 which is on the long-scale response. It is felt that some encouragement for such further research is provided by the present study.

Acknowledgements

Support from DERA and EPSRC, U.K., is gratefully acknowledged, as are the referees' helpful comments.

Appendix A. Direct-simulation method for two-dimensional multi-branching

This appendix outlines the direct numerical method used in the two-dimensional branching problem of Section 4 with prescribed pressures in the mother and each of the daughter tubes. See also [32,33]. The geometry is a single mother upstream between $y = -1$ and $y = 1$ which splits into n equal sized daughters at $x = 0$. The upstream and downstream limits at which the pressures were imposed were taken to be at $x = -1$, $x = 1$ respectively. We make use of the x-momentum equation

$$uu_x + vu_y = -p_x + \frac{1}{\mathrm{Re}}\nabla^2 u, \tag{A1}$$

the Poisson equation for the pressure

$$-\nabla^2 p = 2(u_y v_x - u_x v_y), \tag{A2}$$

and the continuity equation. Here (A1), (A2) are discretised using standard second-order accurate centred differences. Also, in order to avoid evaluating p at the leading edges of the branches, near those edges we skew the grid using the points at $x + y,\ x - y$ instead of x, y. A significant issue in using the continuity equation is that we are aiming to solve a first-order differential equation but with two boundary conditions, *e.g.* $v = 0$ on both the outer walls. We accommodate this by discretising the continuity equation as in [32], effectively solving it as a two-point boundary value problem, together with iteration. Thus the continuity equation becomes

$$3v_{ij-1} - 4v_{ij} + v_{ij+1} = r_i, \tag{A3}$$

where

$$r_i = \frac{1}{3}(u_{i+1,j+1} - u_{i-1,j+1}) + \frac{2}{3}(u_{i-1,j} - u_{i+1,j} - u_{i+1,j-1} + u_{i-1,j-1}) \tag{A4}$$

and i, j refer to grid points in the x, y directions respectively. The boundary conditions $u = v = 0$ on the walls can then be imposed on the normal velocity simply by requiring $v_{ij} = 0$ at both $y = \pm 1$. Upstream, the form

$$u = \frac{Q}{4}(1 + y)(1 - y), \quad v = 0 \tag{A5}$$

is taken as in the high Reynolds number case of Section 4. Downstream, we impose $u_x = 0$. Upstream in the mother and downstream in each daughter the values of the pressure are also prescribed. The wall conditions for the pressure are obtained from (A2) and the known velocity values. This leads to the requirement that

$$p_y = \frac{v_{yy}}{\mathrm{Re}} \quad \text{on the walls.} \tag{A6}$$

An alternative approach which was also implemented exploited (A1) along the walls. We then have a first-order differential equation but with the values of the pressure known at each of the end points. We can therefore solve as for (A3), to obtain the p_{ij} values along the wall from

$$3p_{ij-1} - 4p_{ij} + p_{ij+1} = s_i, \tag{A7}$$

where s_i depends upon the local velocity values. Using this approach on the outer walls proved successful, yielding essentially the same pressure distribution as for (A6). Unfortunately we were unable to achieve the same on the internal divider walls due to the leading edges present. Using this latter method proved more stable however when iterating to obtain the flow solution.

The iteration procedure involved iterating the p and u solutions first, leaving v unchanged. Then p was left unchanged while the current u and v guesses were converged, before the p and u iteration was repeated and so on. This was found in practice to be the most stable way of performing the iterations. After an initial guess, Q is found iteratively by imposing conservation of mass through calculating the total mass flux downstream and setting the next Q guess, so that the mass flux into the mother tube balances the mass flux out through the daughters. As Re was increased, better initial guesses were required to achieve convergence; converged solutions for lower Reynolds number were used. The computations reached Re of

around 100 for some geometries and pressure distributions but considerably lower (60–100) in others.

The results of this method at various Re are compared with the large Re analysis in Figure 7(c). Smaller downstream areas were obtained (*i.e.*, $A < 1$) by simply shutting off some of the downstream area nearest the outer wall, effectively shutting off a daughter tube.

Appendix B. Direct-simulation method in three dimensions

The unsteady three-dimensional incompressible Navier-Stokes equations were solved using a parallel time-accurate finite-volume solver. The solver is capable of dealing with moving boundaries, moving grids and complex three-dimensional vascular systems. The computational domain is divided into multiple block subdomains. At each cross section the plane is divided into twelve sub-zones to allow flexibility for handling complex geometries and, if needed, appropriate parallel data partitioning. A second-order in time and third-order upwind finite volume method for solving time-accurate incompressible flows based on pseudo-compressibility and dual time-stepping technique is used. Performing a series of numerical simulations validated this code. The results of these simulations, representative of typical biological flows, have been compared with theoretical and experimental results.

In the numerical method, the equations in strong conservative form are written in a generalized curvilinear coordinate system, such that

$$\int_{V(t)} \frac{\partial \overline{\mathbf{q}}}{\partial \tau}\,\mathrm{d}V + \frac{\partial}{\partial t}\int_{V(t)} \overline{\mathbf{Q}}\,\mathrm{d}V + \int_{S(t)} \left(\overline{\overline{\mathbf{f}}} - \overline{\mathbf{Q}}\overline{\mathbf{v}}_{\mathbf{g}}\right)\cdot \hat{\mathbf{n}}\,\mathrm{d}S = 0, \tag{B1}$$

where $\overline{\overline{\mathbf{f}}} = (\overline{\mathbf{F}} + \overline{\mathbf{F}}_v,\ \overline{\mathbf{G}} + \overline{\mathbf{G}}_v,\ \overline{\mathbf{H}} + \overline{\mathbf{H}}_v)$ and

$$\overline{\mathbf{Q}} = \begin{bmatrix} u \\ v \\ w \\ 0 \end{bmatrix},\quad \overline{\mathbf{q}} = \begin{bmatrix} u \\ v \\ w \\ p \end{bmatrix},\quad \overline{\mathbf{F}} = \begin{bmatrix} u^2 + p \\ uv \\ uw \\ \beta u \end{bmatrix}, \overline{\mathbf{G}} = \begin{bmatrix} vu \\ u^2 + p \\ vw \\ \beta v \end{bmatrix},\quad \overline{\mathbf{H}} = \begin{bmatrix} wu \\ wv \\ w^2 + p \\ \beta w \end{bmatrix},$$

$$\overline{\mathbf{F}}_v = -\frac{1}{\mathrm{Re}}\begin{bmatrix} 2u_x \\ u_y + v_x \\ u_z + w_x \\ 0 \end{bmatrix},\quad \overline{\mathbf{G}}_v = -\frac{1}{\mathrm{Re}}\begin{bmatrix} v_x + u_y \\ 2v_y \\ v_z + w_y \\ 0 \end{bmatrix},$$

and

$$\overline{\mathbf{H}}_v = -\frac{1}{\mathrm{Re}}\begin{bmatrix} w_x + u_z \\ w_y + v_z \\ 2w_z \\ 0 \end{bmatrix}. \tag{B2}$$

Here t denotes the real physical time, τ is the pseudo time, and β is the pseudo-compressibility coefficient, while $V(t)$ is the time varying volume of the cell, $S(t)$ denotes the surface of the control volume and $\hat{\mathbf{n}}$ is the outward unit normal vector at the surface of the control volume, where $\overline{\mathbf{v}}_g$ is the local velocity of the moving control surface. The term $\overline{\mathbf{q}}$ associated with the pseudo time is designed for an inner sub-iteration at each physical time step and vanishes

when the divergence of velocity is driven to zero so as to satisfy the equation of continuity. For a structured boundary-fitted computational coordinate system (ξ, η, ζ) and a cell-centred finite volume formulation, we can write Equation (B1) in a semi-discrete form for each cell centred at points (i, j, k),

$$\mathrm{St}\frac{\partial}{\partial t}\left[V\overline{\mathbf{Q}}\right]_{ijk} + \overline{\mathbf{R}}_{ijk} + \mathrm{St}V_{ijk}\left(\frac{\partial\overline{\mathbf{q}}}{\partial\tau}\right)_{ijk} = 0. \tag{B3}$$

Here the steady state residual is given by

$$\overline{\mathbf{R}}_{ijk} = \left(\overline{\overline{\mathbf{F}}}+\overline{\overline{\mathbf{F}}}_v\right)_{i+\frac{1}{2},j,k} - \left(\overline{\overline{\mathbf{F}}}+\overline{\overline{\mathbf{F}}}_v\right)_{i-\frac{1}{2},j,k} + \left(\overline{\overline{\mathbf{G}}}+\overline{\overline{\mathbf{G}}}_v\right)_{i,,j+\frac{1}{2},k}$$

$$- \left(\overline{\overline{\mathbf{G}}}+\overline{\overline{\mathbf{G}}}_v\right)_{i,j-\frac{1}{2},k} + \left(\overline{\overline{\mathbf{H}}}+\overline{\overline{\mathbf{H}}}_v\right)_{i,j,k+\frac{1}{2}} - \left(\overline{\overline{\mathbf{H}}}+\overline{\overline{\mathbf{H}}}_v\right)_{i,j,k-\frac{1}{2}.}$$

Also, the modified flux terms are defined as

$$\overline{\overline{\mathbf{F}}}+\overline{\overline{\mathbf{F}}}_v = \left(\overline{\overline{\mathbf{f}}} - St\overline{\mathbf{Q}}\,\overline{\mathbf{v}}_g\right)\cdot\overline{\mathbf{S}}_n^{\xi}, \overline{\overline{\mathbf{G}}}+\overline{\overline{\mathbf{G}}}_v = \left(\overline{\overline{\mathbf{f}}} - St\overline{\mathbf{Q}}\,\overline{\mathbf{v}}_g\right)\cdot\overline{\mathbf{S}}_n^{\eta},$$

$$\overline{\overline{\mathbf{H}}}+\overline{\overline{\mathbf{H}}}_v = \left(\overline{\overline{\mathbf{f}}} - St\overline{\mathbf{Q}}\,\overline{\mathbf{v}}_g\right)\cdot\overline{\mathbf{S}}_n^{\zeta.} \tag{B4}$$

The normal-area vector in the ξ-direction is

$$\overline{\mathbf{S}}_n^{\xi} = \left[S_{nx}^{\xi}, S_{ny}^{\xi}, S_{nz}^{\xi}\right]. \tag{B5}$$

In the above formulation the flow Strouhal number is defined as $\mathrm{St} = D/(U_{\mathrm{ref}}t_{\mathrm{ref}})$. The physical time derivatives are differenced using the second order trapezoidal implicit method, while first order Euler implicit differencing is used on the pseudo-time derivatives. The inviscid fluxes are differenced using third-order upwind implementation of Roe's flux-difference split averaging technique. Second order central differencing is used on the viscous fluxes. To maintain second order spatial accuracy a special treatment at the boundaries is required. For more detail on other aspects of the numerical technique see [34–38].

To generate the branch model (concerning Section 5) and its appropriate grid, a main mother tube of 5 diameters in length from the main inlet to the bifurcation point is chosen. After the bifurcation plane, each daughter tube is also extended by 5 MD (mother tube diameter) to the outlet. In this study, only symmetric bifurcations are considered. However, since we solve over a full grid comprising the entire branch, the method is capable of solving for any nonsymmetry in shape, size, branch angle and any tube differences in general. In all the present examples we only consider the case of splitting the mother tube in half from the centre line by any given half angle. In the mother tubes, we use a $38 \times 51 \times 15$ grid, which implies using 38 cells in the tube axial direction by 51 cells in the azimuthal direction and 15 cells in the radial direction at each cross section of the tube. In each of the daughter tubes a $55\times75\times20$ grid is used. We use appropriate grid stretching near the walls in the radial direction and near the bifurcation region in the axial direction. The above grid was the finest grid used in our grid resolution studies, which assured virtually unnoticeable change from the next coarse grid considered. All the computational results are achieved by allowing the residual on velocities to drop to 10^{-16} and the residual on mass conservation drop to 10^{-13}.

References

1. M.R. Roach, S. Scott and G.G. Ferguson, The hemodynamic importance of the geometry of bifurcations in the circle of Willis glass model studies. *Stroke* 3 (1972) 255–267.
2. M. Motimoya and T. Karino, Flow patterns in the human carotid artery bifurcation. *Stroke* 15 (1984) 50–55.
3. M. Fisher and S. Fieman, Geometric factors of the bifurcation in carotid atherogenesis. *Stroke* 21 (1990) 267–271.
4. M.J. Lighthill, Physiological fluid dynamics: a survey. *J. Fluid Mech.* 52 (1972) 475–497.
5. T. Handa, M. Negoro, S. Miyachi and K.Sugita, Evaluation of pressure changes in feeding arteries during embolization of intracerebral arteriovenous malformations. *J. Neurosurg.* 79 (1993) 383–389.
6. G.J. Hademonos and T.F. Massoud, Biophysical mechanisms of stroke. *Stroke* 28 (1997) 2067–2077.
7. Y. Miyasaka, K. Yada, A. Kurata, K. Tokiwa, K. Irikura, R. Tanaka, T. Ohwada and T. Kitahara, Correlation between intravascular pressure and risk of haemorrhage due to arteriovenous malformations. *Surg. Neurol.* 39 (1993) 370–373.
8. W.L. Young, A. Kader, J. Pile-Spellman, E. Ornstein and B.M. Stein, Arteriovenous malformation drawing vein physiology and determinants of transnidal pressure gradients. *Neurosurgery* 35 (1996) 389–396.
9. F.T. Smith and M.A. Jones, AVM modelling by multi-branching tube flow: large flow rates and dual solutions. *IMA J. Math. Med. Biol.* (2003) in press.
10. T.J. Pedley, Pulmonary fluid dynamics. *Ann. Rev. Fluid Mech.*, 9 (1997), 229–274; also T.J. Pedley, R.C. Schroter, M.F. Sudlow, The prediction of pressure drop and variation of resistance within the human bronchial airways. *Respir. Physiol.* 9 (1970) 387–405.
11. F.T. Smith, Steady motion through a branching tube. *Proc. R. Soc. London* A 355 (1977) 167–187.
12. J. Bennett, *Theoretical Properties of Three-Dimensional Interactive Boundary Layers.* PhD thesis, University of London (1987) 150pp.
13. A.G. Walton and F.T. Smith, Concerning three-dimensional flow past a tall building on flat ground. *Q.J. Mech. Appl. Maths.* 50 (1997) 97–128.
14. C.G. Caro, D.J. Doorly, M. Tarnawski, K.T. Scott, Q. Long and C.L. Dumoulin, Non-planar curvature and branching of arteries and non-planar type flow. *Proc. R. Soc. London* A 452 (1996) 185–197.
15. M.G. Blyth and A.J. Mestel, Steady flow in a dividing pipe. *J. Fluid Mech.* 401 (1999) 339–364.
16. G.J. Hademonos, T.F. Massoud and F. Vinuela, A biomathematical model of intracranial arteriovenous malformations based on electrical network analysis: theory and hemodynamics. *Neurosurgery* 38 (1996) 1005–1015.
17. E. Gao, W.L. Young, J. Pile-Spellman, S. Joshi, H. Duong, P.E. Stieg and Q. Ma, Cerebral arteriovenous malformation feeding artery aneurysms; a theoretical model of intravascular pressure changes after treatment. *Neurosurgery* 41 (1997) 1345–1358.
18. J.K. Comer, C. Kleinstreuer and Z. Zhang, Flow structures and particle deposition patterns in double-bifurcation airway models. Part 1. Air flow fields. *J. Fluids* 435 (2001) 25–54.
19. B. Gatlin, C. Cuichi, J. Hammersley, D. Olson, R. Reddy and G. Burnside, Computational simulation of steady and oscillating flow in branching tubes. *Bio-Med. Fluids Eng. ASME FED* 212 (1995) 1–8.
20. Y. Zhao, C.T. Brunskill and B.B. Lieber, 1997, Inspiratory and expiratory steady flow analysis in a model symmetrically bifurcating airway. *Trans. ASME J. Biomech. Eng.* 119 (1997) 52–65.
21. F. Wilquem and G. Degrez, Numerical modelling of steady inspiratory airflow through a three-generation model of the human central airways. *J. Biomech. Engng.* 119 (1997) 59–65.
22. B. Snyder, D.R. Dantzker and M.J. Jaeger, Flow partitioning in symmetric cascades of branches. *J. Appl. Physiol.* 51 (1981) 598–606.
23. C. Raick, A. Ramuzat, P. Corieri and M.L. Riethmuller, Numerical and experimental study of spatial periodicity of steady air flows in pulmonary bifurcations. In: G.M. Carlomagno and I. Grant (eds.), *Proceedings of the 7th Triennial International Symposium on Fluid Control.* Sorrento, Italy, Aug. 25–28 (2003) in press.
24. T.J. Pedley, R.C. Schroter and M.F. Sudlow. In: J.B. West (ed.), *Bioengineering Aspects of the Lung.* New York: Dekker (1997) pp. 163–265.
25. T.J. Pedley, In: The Fluid Mechanics of Large Blood Vessels, Ch.5: flow patterns and wall shear stress in arteries, III, Branched tubes and flow instability. Cambridge Univ. Press (1980) 446 pp.
26. M. Lei, C. Kleinstreuer and J.P. Archie, Hemodynamic simulations and computer-aided designs of graft-artery junctions. *J. Biomech. Engng.* 119 (1997) 343–348.

27. F.T. Smith, N.C. Ovenden, P. Franke and D.J. Doorly, What happens to pressure when a flow enters a side branch? *J. Fluid Mech.* 479 (2003) 231–258.
28. F.T. Smith and M.A. Jones, One-to-few and one-to-many branching tube flows. *J. Fluid Mech.* 423 (2000) 1–31.
29. F.T. Smith, On flow through bends and branchings *Biorheology* 39 (2002) 373–378.
30. R. Purvis, R.I. Bowles, S.C.R. Dennis and F.T. Smith, Direct computational solutions and comparisons for one-to-many branching tube flows. (2003) in preparation.
31. M. Tadjfar and F.T. Smith, Direct simulations and modelling of basic three-dimensional tube flows. Submitted, *J. Fluid Mech.* (2003).
32. S.C.R. Dennis and J.D. Hudson, Methods of solution of the velocity-vorticity formulation of the Navier-Stokes equations. *J. Comp. Phys.* 122 (1995) 300–306.
33. J.S. Bramley and S.C.R. Dennis, The numerical solution of two-dimensional flow in a branching channel. *Comp. Fluids* 12 (1984) 339–355.
34. M. Tadjfar and R. Himeno, Time-accurate, parallel, multi-zone, multi-block solver to study the human cardio-vascular system. *Biorheology* 39 (2002) 379–384.
35. M. Tadjfar and R. Himeno, Parallel, multi-zone, multi-block solver to study arterial branches in the human vascular system. In: U.S. Rohatgi (ed.), *Proceedings of the ASME Fluids Engineering Division*, Vol. 256. New York: ASME (2001) pp. 357–364.
36. M. Tadjfar, T. Yamaguchi and R. Himeno, Parallel solver for blood flow in human vascular system. In: T.J. O'Hern (ed.), *Proceedings of the ASME Fluids Engineering Division*, Vol. 253. New York: ASME (2000) pp. 567–572.
37. H. Liu and K. Kawachi, A numerical study of insect flight. *J. Comp. Phys.* 146 (1998) 124–156.
38. S.E. Rogers and D. Kwak, Upwind differencing scheme for the time-accurate incompressible Navier-Stokes equations. *AIAA J.* 28 (1990) 253–262.